NON-DISSOCIATIVE SINGLE-ELECTRON CAPTURE BY CO^{2+} FROM RARE GASES

Z. HERMAN [1], P. JONATHAN, A.G. BRENTON and J.H. BEYNON
Mass Spectrometry Research Unit, Department of Chemistry, University College of Swansea, Swansea SA2 8PP, UK

Received 15 May 1987; in final form 15 September 1987

The state-selective non-dissociative single-electron capture reactions of 6 keV CO^{2+} ions from rare gas (He, Ne, Ar, Kr, Xe) targets are investigated by translational energy spectroscopy. Capture from $CO^{2+}(^3\Pi)$ into doublet states of CO^+ dominates. However, there are firm indications for the involvement of electronically excited CO^{2+} (1.7 eV above $CO^{2+}(^3\Pi)$) in the projectile beam, and also for the formation of quartet states of CO^+. Landau–Zener reaction windows, derived specifically for atomic ion–atom systems, are applied to this diatomic dication–atom series, giving excellent agreement with experiment.

1. Introduction

The elementary charge transfer reactions of multiply charged atomic ions and atoms have been the subject of extensive research in recent years. A considerable body of data on total cross sections for these processes has been obtained, over a wide range of impact energies, from thermal and sub eV collisions [1,2] to the keV domain [3,4]. Application of single collision methods with product energy analysis (translational energy spectroscopy [5,6], scattering [6,7]) has offered information on total and differential cross sections for state selective processes. Besides atomic targets, molecular targets have been investigated in some instances [8,9]. Single-electron capture by multiply charged molecular ions has attracted attention lately [10,11].

The present investigation involves the non-dissociative state-selective single-electron capture reactions of doubly-charged diatomic ions, i.e. processes of the type:

$$\overrightarrow{AB^{2+}} + C \rightarrow \overrightarrow{AB^{+}} + C^{+} \qquad (1)$$

in the keV collision energy range using translational spectroscopy. Studies of this nature are of considerable value:

(a) They provide relative cross section data for state-to-state molecular processes (1), and populations of the various product electronic states; this information is equally important for atomic and molecular systems in determining the ionised structure of highly energised species.

(b) For atomic systems, the fast product energy is either electronic or translational. For molecular projectiles, however, part of the energy made available by the electron transfer may be deposited in product vibration and rotation; the overall energy balance of process (1) (in the centre of mass frame) can be written as

$$E_{tr} = E_i(AB^{2+}) + E_{exc}(AB^{2+}) - [E_i(AB^{+}) + E_{exc}(AB^{+}) + E_i(C^{+})], \qquad (2)$$

where E_{tr} is the relative translational energy of the products and $E_i(AB^+)$, $E_i(AB^{2+})$ are the ionisation energies for formation of the participating electronic state ($v=J=0$) of AB^+ and AB^{2+}, respectively, from ground state ($v=J=0$) neutral AB. Similarly, $E_i(C^+)$ denotes the ionisation energy of the target atom C to its final cationic state. $E_{exc}(AB^+)$, $E_{exc}(AB^{2+})$ are the internal (vibrational and rotational) excitation energies of AB^+ and AB^{2+} respectively; the recombination energy $E_R(AB^{2+}–AB^+)$ is thus $E_{tr}+E_i(C^+)$.

(c) The energy levels of reactant dications (stable

[1] Royal Society–Czechoslovak Academy of Sciences Exchange Scientist 1986. Permanent address: J. Heyrovský Institute of Physical Chemistry and Electrochemistry, Czechoslovak Academy of Sciences, Máchova 7, 121 38 Prague 2, Czechoslovakia.

on the mass spectrometer timescale) may be obtained from their recombination energies, as reflected in translational energy spectra. In the present experiments, information on energetics and spectroscopic assignment of molecular dications is not entirely clear in some cases; their participation in process (1), studied as described here, indicates that their mean lifetimes are longer than $\approx 10^{-5}$ s.

In the present communication, we explore single-electron capture by doubly charged carbon monoxide ions from rare gas atoms:

$$\overrightarrow{CO^{2+}} + R \rightarrow \overrightarrow{CO^{+}} + R^{+}, \quad (3)$$

where R = He, Ne, Ar, Kr, Xe. The laboratory translational energy of CO^{2+} was fixed at 6 keV.

The ionisation energy (CO–CO^{2+}) has been measured by several authors [12–15]. The average value of these determinations is 41.5 ± 0.4 eV. Theoretical calculations [16,17] of potential energy curves for CO^{2+}, based on the semi-empirical procedure due to Hurley [16], have been performed. Curtis and Boyd [17] used their calculations to explain experimental results for spontaneous and collision-induced dissociation of CO^{2+}. Recently, a very thorough theoretical treatment of CO^{2+} has been published [18]. Data relevant to the current investigation is summarised in table 1. In particular, we have assumed $CO^{2+}(^3\Pi)$ (equilibrium internuclear separation, $R_e \approx 1.2$ Å) to be the lowest quasi-bound state of CO^{2+}, despite the fact that $CO^{2+}(^3\Sigma^-)$ has a calculated [18] minimum (at $R_e \approx 1.7$ Å) ≈ 4.1 eV lower than $CO^{2+}(^3\Pi)$. However, since the Franck–Condon region for formation of CO^{2+} by electron impact of CO also lies at ≈ 1.2 Å, then pop-

Table 1
Ionisation energy data

Ion	State	E_i (eV)	Equilibrium internuclear separation (Å)
CO^{2+}	$^3\Pi$	41.5 ± 0.4 [12–15] 40.1 [17] 41.1 [18]	1.18 [18]
	$^1\Pi$	42.5 [16,17] 41.74 [18]	1.15 [18]
	$^1\Sigma^+$	42.05 [18]	1.1 [18]
CO^+ [19]	$X\,^2\Sigma^+$	14.01	1.115
	$A\,^2\Pi$	16.54	1.244
	$B\,^2\Sigma^+$	19.68	1.168
	$C\,^2\Delta$	21.83	1.346
	$D\,^2\Pi$	22.10	(1.25)
	$(G\,^2\Sigma$	23.09)	
	$E\,^2\Sigma$	24.82	(1.21)
	$F\,^2\Sigma$	27.12	
He^+ [20]	$^2S_{1/2}$	24.59	–
Ne^+ [20]	$^2P_{3/2}$	21.56	–
Ar^+ [20]	$^2P_{3/2}$	15.76	–
Kr^+ [20]	$^2P_{3/2}$	14.00	–
	$^2P_{1/2}$	14.67	–
Xe^+ [20]	$^2S_{1/2}$	27.47	–
	$^2P_{3/2}$	12.13	–
	$^2P_{1/2}$	13.44	–
	$^2S_{1/2}$	23.39	–

ulation of $CO^{2+}(^3\Sigma^-)$ by this process is extremely unlikely (as it leads to dissociation). Further, the fully allowed [18] radiative dipole $CO^{2+}(^3\Pi) \rightarrow CO^{2+}(^3\Sigma^-)$ transition will also result in dissociation; that is, the $CO^{2+}(^3\Sigma^-)$ so formed will not survive to the interaction region of our apparatus (necessitating a lifetime on the microsecond timescale). Again, electron capture by $CO^{2+}(^3\Sigma^-)$ ($R_e \approx 1.7$ Å) to low-lying CO^+ states (with $R_e \approx 1.2$ Å (see table 1)) is improbable from consideration of the Franck–Condon principle.

Spectroscopic information on CO^+ is plentiful. The three lowest states are firmly established, with photoelectron studies providing information on higher doublet states. We use the standard compilation of Huber and Herzberg [19] (table 1). For completeness, table 1 also gives the ionisation energies of the rare gas target atoms [20] used in calculating exothermicities for the processes under consideration.

2. Experimental

Experiments were conducted with the ZAB-2F reversed-geometry double-focusing mass spectrometer [21]. The experimental procedure has been described elsewhere [9]. Briefly, carbon monoxide dications are produced by 100 eV electron impact on CO gas, in the ionisation chamber of the conventional Nier-type ion source, extracted and accelerated to 6 keV translational energy. The CO^{2+} ions, mass selected by a sector magnet, enter a collision cell (2 cm long) located at the intermediate focal point of the mass spectrometer, containing target gas at a pressure of ≈ 0.2 Pa. Translational energy spectra are obtained under high-resolution conditions, by scanning the voltage applied to the plates of the cylindrical electrostatic analyser, located after the collision cell. The energy resolution on the primary beam is ≈ 0.2 eV (fwhm); for product CO^+ spectra, the energy resolution, estimated from earlier studies of atomic ion–atom systems [9], is ≈ 1 eV.

Calibration of the absolute energy scale, an essential preliminary to accurate interpretation of translational energy spectra, facilitates precise measurement of exothermicities for the observed state-selective capture processes. This calibration was performed by means of an internal standard: a small amount of argon gas was added to the carbon monoxide source sample, in order that spectra for the Ar^{2+}–rare-gas charge transfer reactions,

$$\overrightarrow{Ar^{2+}} + R \rightarrow \overrightarrow{Ar^{+}} + R^+, \qquad (4)$$

could be measured repeatedly, before and after each run of the corresponding CO^{2+}–rare-gas system (3). Since the translational energy spectra for processes (4) are well known [9], a reliable procedure for energy scale calibration is established. For the spectra herein, a correction offset of 5.5 ± 0.2 eV was necessary.

3. Results

Translational energy spectra for CO^+ ions formed in collisions of CO^{2+} with He, Ne, Ar and Kr, Xe are shown in figs. 1 and 2 respectively. The abscissa scale is given in terms of the translational exothermicity ΔE of process (3) in question, defined by

$$\Delta E = E_{lab}(CO^+) - E_{lab}(CO^{2+}). \qquad (5)$$

Under the conditions of translational energy spectroscopy experiments (i.e. projectile laboratory translational energy is much greater than the exothermicity of the collision process in question; scattering angle approaching zero), the translational exothermicity ΔE can be equated to the translational energy release E_{tr} (eq. (2)) of process (1). The translational energy scale was accurately calibrated (± 0.2 eV) by the technique described above. Exothermicities ΔE_0 for competing capture processes are given in figs. 1 and 2, and in detail in table 2; ΔE_0 is calculated assuming no vibrational excitation of molecular ions. Peak positions are consistent with a value of 27.0 eV for the recombination energy $E_R(CO^{2+}\text{–}CO^+(X\,^2\Sigma^+))$; consequently, this value was used as the ionisation energy of CO^+, for calculating ΔE_0 in table 2. Our experimentally determined value of 41.0 ($=27.0+14.0$) eV for the vertical double-ionisation energy of CO is in good agreement with the data displayed in table 1 for the energy to form the zeroth vibrational level of $CO^{2+}(^3\Pi)$.

Designation of particular processes is greatly simplified by adopting a modified version of Hasted's notation [22]: Greek letters α, β, γ, ... indicate the

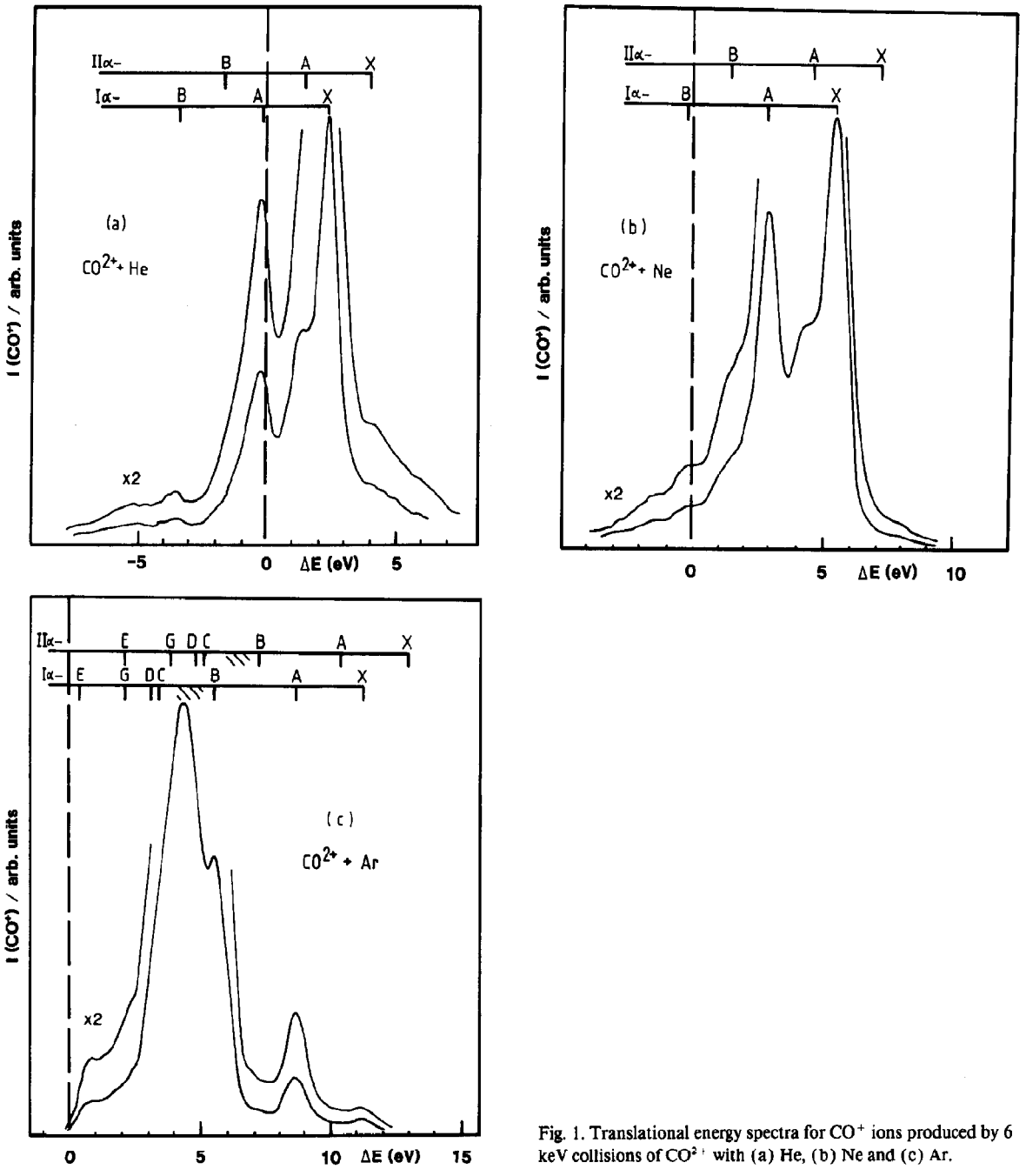

Fig. 1. Translational energy spectra for CO^+ ions produced by 6 keV collisions of CO^{2+} with (a) He, (b) Ne and (c) Ar.

ground and successive states of the atomic (rare gas) ion R^+, whereas Roman numerals (I, II, III, ...) and Arabic letters (X, A, B, ...) are reserved for the fast projectile states of CO^{2+} (i.e. I ⇔ $CO^{2+}(^3\Pi)$) and CO^+ respectively. Each particular reaction channel is detailed in table 2.

3.1. CO^{2+}–He

The translational energy spectrum for this system (fig. 1a) is easily interpreted. The main peak corresponds to the process IαX (table 2). The other ob-

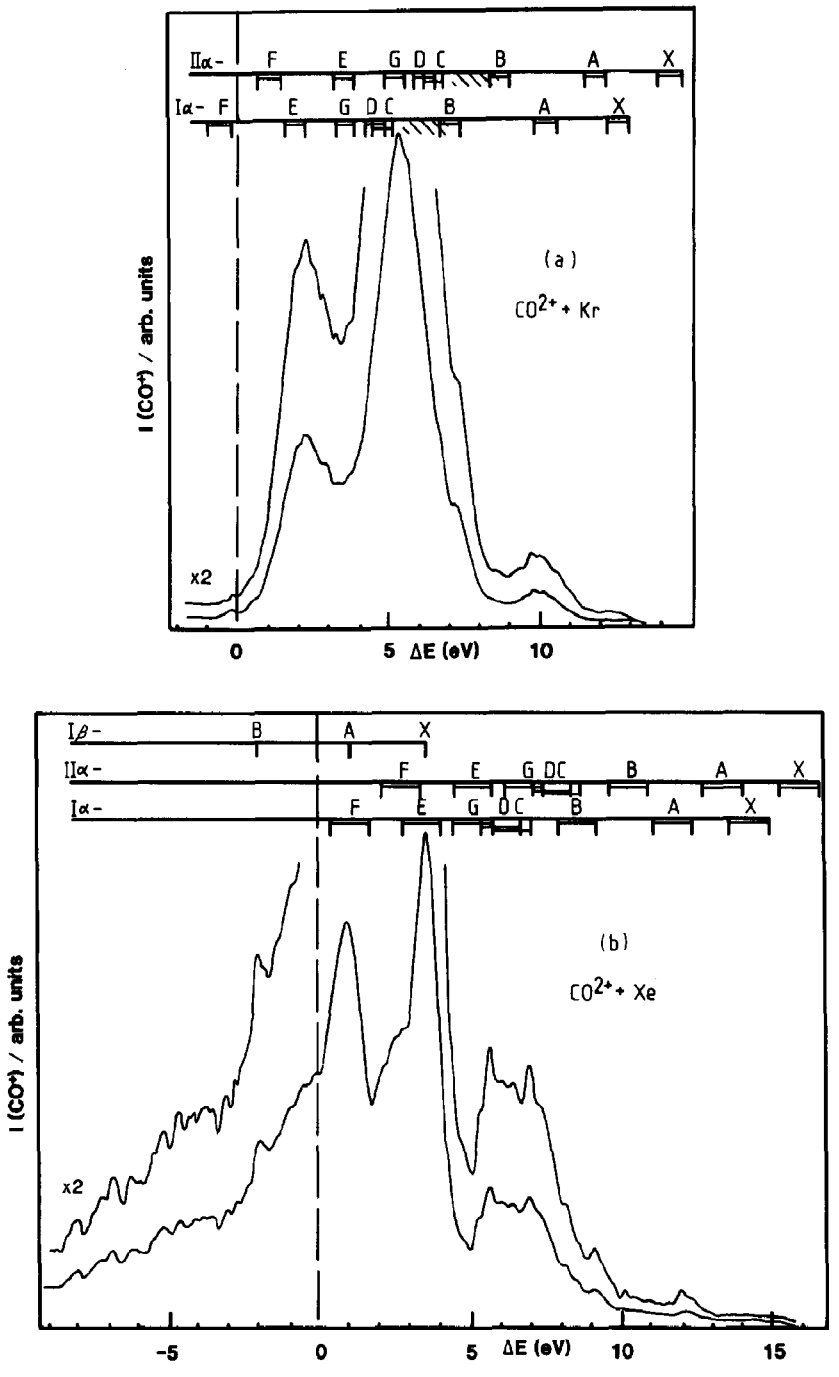

Fig. 2. Translational energy spectra for CO^+ ions produced by 6 keV collisions of CO^{2+} with (a) Kr and (b) Xe.

servable process is the almost thermoneutral formation of $CO^+(A\,^2\Pi)$, whereas the endothermic channel IαB is barely visible. The position of the peaks in the calibrated absolute energy scale is consistent with a recombination energy $E_R(CO^{2+}$–$CO^+(X\,^2\Sigma^+))$ equal to 27.0 eV. Reaction channels involving a higher-lying excited state of CO^{2+} are indicated by peaks IIαX and, more clearly, IIαA. The

Table 2
Exothermicities of reaction channels [a)]

	ΔE_0 (eV)	Designation
$CO^{2+}(^3\Pi)+He(^1S_0)\rightarrow CO^+(X^2\Sigma^+)+He^+(^2S_{1/2})$	2.40	IαX
$\rightarrow CO^+(A^2\Pi)+He^+(^2S_{1/2})$	−0.12	IαA
$\rightarrow CO^+(B^2\Sigma^+)+He^+(^2S_{1/2})$	−3.26	IαB
$CO^{2+*}+He(^1S_0)\rightarrow CO^+(X^2\Sigma^+)+He^+(^2S_{1/2})$	4.10	IIαX
$\rightarrow CO^+(A^2\Pi)+He^+(^2S_{1/2})$	1.58	IIαA
$\rightarrow CO^+(B^2\Sigma^+)+He^+(^2S_{1/2})$	−1.56	IIαB
$CO^{2+}(^3\Pi)+Ne(^1S_0)\rightarrow CO^+(X^2\Sigma^+)+Ne^+(^2P_{3/2})$	5.42	IαX
$\rightarrow CO^+(A^2\Pi)+Ne^+(^2P_{3/2})$	2.90	IαA
$\rightarrow CO^+(B^2\Sigma^+)+Ne^+(^2P_{3/2})$	−0.24	IαB
$CO^{2+*}+Ne(^1S_0)\rightarrow CO^+(X^2\Sigma^+)+Ne^+(^2P_{3/2})$	7.12	IIαX
$\rightarrow CO^+(A^2\Pi)+Ne^+(^2P_{3/2})$	4.60	IIαA
$\rightarrow CO^+(B^2\Sigma^+)+Ne^+(^2P_{3/2})$	1.46	IIαB
$\rightarrow CO^+(C^2\Delta)+Ne^+(^2P_{3/2})$	−0.69	IIαC
$CO^{2+}(^3\Pi)+Ar(^1S_0)\rightarrow CO^+(X^2\Sigma^+)+Ar^+(^2P_{3/2})$	11.23	IαX
$\rightarrow CO^+(A^2\Pi)+Ar^+(^2P_{3/2})$	8.70	IαA
$\rightarrow CO^+(B^2\Sigma^+)+Ar^+(^2P_{3/2})$	5.57	IαB
$\rightarrow CO^+(C^2\Delta)+Ar^+(^2P_{3/2})$	3.41	IαC
$\rightarrow CO^+(D^2\Pi)+Ar^+(^2P_{3/2})$	3.14	IαD
$\rightarrow CO^+(G^2\Sigma)+Ar^+(^2P_{3/2})$	2.15	IαG
$\rightarrow CO^+(E^2\Sigma)+Ar^+(^2P_{3/2})$	0.12	IαE
$\rightarrow CO^+(F^2\Sigma)+Ar^+(^2P_{3/2})$	−1.88	IαF

	ΔE_0 (eV)		Designation
	$j=3/2$	$j=1/2$	
$CO^{2+}(^3\Pi)+Kr(^1S_0)\rightarrow CO^+(X^2\Sigma^+)+Kr^+(^2P_j)$	13.00	12.32	IαX
$\rightarrow CO^+(A^2\Pi)+Kr^+(^2P_j)$	10.47	9.80	IαA
$\rightarrow CO^+(B^2\Sigma^+)+Kr^+(^2P_j)$	7.34	6.67	IαB
$\rightarrow CO^+(C^2\Delta)+Kr^+(^2P_j)$	5.17	4.50	IαC
$\rightarrow CO^+(D^2\Pi)+Kr^+(^2P_j)$	4.90	4.23	IαD
$\rightarrow CO^+(G^2\Sigma)+Kr^+(^2P_j)$	3.91	3.24	IαG
$\rightarrow CO^+(E^2\Sigma)+Kr^+(^2P_j)$	2.18	1.51	IαE
$\rightarrow CO^+(F^2\Sigma)+Kr^+(^2P_j)$	−0.12	−0.79	IαF
$CO^{2+}(^3\Pi)+Xe(^1S_0)\rightarrow CO^+(X^2\Sigma^+)+Xe^+(^2P_j)$	14.86	13.55	IαX
$\rightarrow CO^+(A^2\Pi)+Xe^+(^2P_j)$	12.33	11.02	IαA
$\rightarrow CO^+(B^2\Sigma^+)+Xe^+(^2P_j)$	9.20	7.89	IαB
$\rightarrow CO^+(C^2\Delta)+Xe^+(^2P_j)$	7.04	5.73	IαC
$\rightarrow CO^+(D^2\Pi)+Xe^+(^2P_j)$	6.77	5.46	IαD
$\rightarrow CO^+(G^2\Sigma)+Xe^+(^2P_j)$	5.78	4.47	IαG
$\rightarrow CO^+(E^2\Sigma)+Xe^+(^2P_j)$	4.05	2.74	IαE
$\rightarrow CO^+(F^2\Sigma)+Xe^+(^2P_j)$	1.75	0.44	IαF
$\rightarrow CO^+(X^2\Sigma^+)+Xe^{+*}(^2S_{1/2})$	3.61		IβX
$\rightarrow CO^+(A^2\Pi)+Xe^{+*}(^2S_{1/2})$	1.08		IβA
$\rightarrow CO^+(B^2\Sigma^+)+Xe^{+*}(^2S_{1/2})$	−2.05		IβB

[a)] Exothermicities of CO^{2+*} (channels IIα⁻) are 1.7 eV larger than the corresponding Iα⁻ process.

state can be placed at ≈ 1.7 eV above $CO^{2+}(^3\Pi)$, i.e. at 42.7 eV, but its assignment is not obvious (see section 4). Its population in the CO^{2+} projectile beam appears to be fairly small (only a few percent), due to either a low probability of formation in the ionisation process, or dissociation prior to detection.

The overall cross section for capture by CO^{2+} from He is several times smaller than for the other targets examined. For this reason, the unresolved hump at the far right-hand side of fig. 1a, caused by charge transfer from residual background gas, possibly N_2, O_2, CO or H_2O [10], is observed. This feature is only visible for helium target.

3.2. CO^{2+}–Ne

The CO^+ spectrum (fig. 1b) is rather similar to that for CO^{2+}–He, the main process being IαX, exhibiting a slightly asymmetric profile. The relative abundance of IαA, exothermic now by 2.9 eV (table 2) is more than doubled, whereas the endothermic IαB shows a small increase, with respect to IαX. Reactions of the CO^{2+} excited state can be seen as shoulders on the IαX, IαA peaks, due to IIαX, IIαA, shifted from the former by 1.7 eV towards higher ΔE, respectively.

3.3. CO^{2+}–Ar

For this system (fig. 1c), processes IαX and IαA are very exothermic (with ΔE values of 11.23 and 8.7 eV respectively). Reaction channels, favoured by "reaction window" considerations (see section 4), lead to the formation of highly electronically excited CO^+ (mainly in the B, C and D states). The maximum of the translational energy distribution occurs at an exothermicity of ≈ 4 eV, between the calculated locations for processes IαB and IαC, IαD. This maximum cannot be attributed to a strong contribution from reaction channels involving the excited CO^{2+} (namely IIαC, IIαD and IIαG), since our results for He and Ne targets imply that their contributions to the CO^+ spectrum, for processes of comparable ΔE, should be minor. Instead, it is plausible to explain the maximum at $\Delta E \approx 4$ eV as being due to the formation of quartet CO^+ states ($^4\Sigma$ in particular). The latter states have been shown [23–25], by electron impact and collision studies, to lie between 20 and 21 eV above the ground state neutral CO. Spectroscopic information on these quartet states is sparse, however. For the single-electron capture system $CO^{2+}(^3\Pi)$–Ar, the formation of quartet states is spin allowed, and the exothermicities for such processes are favourable. In fig. 1c, their expected ΔE locations are indicated by cross-hatched areas.

3.4. CO^{2+}–Kr

In comparison with the CO^+ spectrum for CO^{2+}–Ar, the CO^{2+}–Kr spectrum (fig. 2a) shows the highly exothermic channels IαX and IαA at lower relative intensities, whereas the IαE channel ($\Delta E = 2.2$–2.8 eV) assumes greater significance. Spin–orbit splitting for Kr^+ (0.66 eV for the $^2P_{3/2}$–$^2P_{1/2}$ states) is manifested by peak broadening. Together with IαC and IαD, processes leading to CO^+ quartet states (translational energy distribution maxima at $\Delta E = 5$–6 eV) are observed, as for CO^{2+}–Ar. No target excitation to Kr^{+*} is visible due to the endothermicity of the reaction

3.5. CO^{2+}–Xe

The spectrum (fig. 2b) is quite complicated. For the Iα– series, channels leading to the CO^+ states C, D, E, F and presumably G dominate. Furthermore, fairly large spin–orbit splittings (1.31 eV) may be inferred from the structure recorded. However, the main peaks in the spectrum relate to processes in which electronically excited $Xe^{+*}(^2S)$ is formed (channels IβX and IβA). Among the endothermic processes, IβB may be identified, but further analysis of the complicated structure for $\Delta E < 0$ is difficult. Processes involving excited CO^{2+} (IIα–, IIβ– series) cannot be reliably assigned.

4. Discussion

Positions of resolved peaks in the translational energy spectra for the systems examined are consistent with a recombination energy $E_R(CO^{2+}$–$CO^+(X\,^2\Sigma^+))$ of 27.0 eV. Assuming population of the ground vibrational level of $CO^+(X\,^2\Sigma^+)$ then this result provides a value of (27.0+14.0) 41.0 eV for

the vertical double-ionisation energy of CO, only slightly lower than the average value of 41.5 ± 0.4 eV from earlier measurements [12–15]. Therefore we conclude that our data correspond, within experimental accuracy, to the energy required for formation of the lowest quasi-bound electronic state of CO^{2+}. Theoretical calculations [16–18] provide the spectroscopic assignment of this state as $CO^{2+}(^3\Pi)$. This agrees with the present findings, in that spin-allowed transitions from $CO^{2+}(^3\Pi)$ to CO^+ quartet states are possible, explaining the translational energy spectra, for Kr and Xe targets in particular.

However, the most accurate recent calculation [18] assumes that the lowest vibrational levels of the $CO^{2+}(^3\Pi)$ state are predissociated by the low-lying $^3\Sigma^-$ state, so that the measured appearance energies [12–15] for CO^{2+} by electron impact of CO are due to formation of quasi-bound $CO^{2+}(^3\Pi, v=2)$ or possibly $CO^{2+}(^1\Pi, v=0)$; consequently, the literature values will be ≈ 0.5 eV higher than the actual $CO(X\,^1\Sigma^+) \rightarrow CO^{2+}(^3\Pi, v=0)$ transition energy. However, $CO^{2+}(^3\Pi, v=0)$ is probably exempt from this fully allowed $CO^{2+}(^3\Pi) \rightarrow CO^{2+}(^3\Sigma^-)$ transition, since $CO^{2+}(^3\Pi, v=0)$ lies below [18] the crossing point of the two participating potential energy curves.

The nature of the higher non-dissociative state of CO^{2+}, contributing to our CO^{2+}–He and CO^{2+}–Ne spectra, lying 1.7 eV above $CO^{2+}(^3\Pi)$ is not clear: Initial calculations [16,17] make the $^1\Pi$ state a good candidate (table 1), but Wetmore et al. [18] place this state much nearer $CO^{2+}(^3\Pi)$, beyond the resolving limit of our apparatus, in fact. For the present experiments, energy resolution (≈ 1 eV) does not permit the detection of possible vibrational structures in our spectra (figs. 1 and 2). However, spin–orbit splitting of the product rare gas ion is apparent as a broadening in the Kr and Xe spectra (fig. 2).

Assuming an interaction distance of ≈ 5 Å, the collision time for a 6 keV CO^{2+} ion with a thermal ground state atom is almost an order of magnitude smaller than the typical vibrational period of the molecular ion. In the most elementary of models, we suppose that transitions leading to exothermic channels occur near crossings of relevant potential energy surfaces. At the crossing point, we further assume that the potential energy curves for CO^{2+} and CO^+ are not perturbed by the presence of the third particle. (This will be more likely for crossings at large interreactant separations.) We expect strong perturbations would show as broadening and shifts of the peaks in translational energy spectra. A schematic example, for the CO^{2+}–Ne system, is given in fig. 3, consisting of the potential energy curves for $(CO\text{–}Ne)^{2+}$ assuming a fixed C–O bond length (fig. 3a), and the potential curves for CO^{2+} and CO^+ with Ne (or Ne^+) infinitely separated (fig. 3b). With reference to the right-hand side curves, it is clear that vertical transitions from the lowest vibrational levels of $CO^{2+}(^3\Pi)$ can qualitatively account for the observed processes IαX and IαA. The peak profiles for the latter processes are drawn on the far right-hand side (fig. 3c); both peaks are narrow and unshifted, with IαX exhibiting a low energy tail.

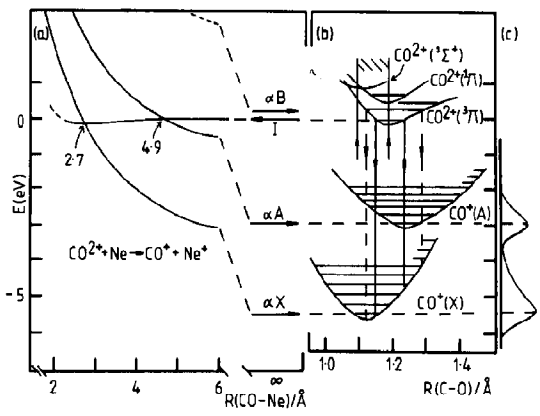

Fig. 3. Schematic potential energy curves, and translational energy release distributions, for CO^{2+}–Ne collisions. (a) Potential energy curves for $(CO\text{–}Ne)^{2+}$ assuming fixed C–O bond length. (b) Potential energy curves for CO^{2+} and CO^+ (with Ne or Ne^+) at infinite interreactant separation. (c) Predicted translational energy distribution of CO^+ product ions.

An approximate rule [1] for determining relative cross sections for atomic ion–atom capture processes states that cross sections are large when crossings of the diabatic potential energy curves for the incoming and outgoing systems occur in a "reaction window" of internuclear distance (≈ 2–6 Å). This, in turn, corresponds to exothermicities ΔE for the state selective processes of ≈ 2–7 eV. Such a rough estimate holds if the size of the cross section is determined mainly by Landau–Zener-type transitions in the vicinity of the crossing point. For molecular systems

of type (1), the situation is, of course, far more complex: in triatomic systems, crossing seams of potential energy surfaces are involved in general. It is also possible that crossings of large families of vibrationally adiabatic surfaces may be significant, together, at higher collision energies, with multisurface crossings. Nevertheless, to a first approximation, an analogous rule may be observed in our results. Kimura et al. [26] define the reaction window for atomic ion–atom charge transfer in terms of a transmission coefficient T derived from the semi-classical Landau–Zener analysis:

$$T(\gamma)=4\int_1^\infty t^{-3}[\exp(-\gamma t)-\exp(-2\gamma t)]\,\mathrm{d}t. \qquad (6)$$

For sufficiently large crossing distances, the function γ takes the form

$$\gamma=4.25\times10^{11}(\Delta E^2 v)^{-1}f^2$$
$$\times\exp[-13.8(\Delta E)^{-1}E_i^{1/2}(\mathrm{R}^+)], \qquad (7)$$

where v is the impact velocity (m s^{-1}) and ΔE, $E_i(R^+)$ are expressed in eV. The constant f, defined in terms of the principal quantum numbers of the resultant electronic state of the fast product, has values $0<f\leqslant1$. For the present comparison, the value of f is taken to be unity; a smaller value ($f<1$) shifts the window towards larger exothermicity. Using eqs. (6) and (7), reaction windows for 6 keV CO^{2+}–rare-gas systems were calculated. For ease of discussion, the windows are parameterised [9] in terms of the set (M, L–H) of exothermicity ΔE (eV) at which $T(\gamma)$ maximises (M), and the range (L–H) over which $T(\gamma)>0.2M$. Results are displayed in table 3.

Table 3
Parameterised reaction windows for 6 keV CO^{2+}–rare-gas single-electron capture systems

Target atom	Reaction window (eV)
He	(5.7, 4.5–6.9)
Ne	(5.3, 4.2–6.4)
Ar	(4.4, 3.5–5.2)
Kr	(4.1, 3.3–4.9)
Xe	(3.7, 3.0–4.5)

Maxima of the experimentally measured translational energy distributions (figs. 1 and 2) are in excellent agreement with calculations (table 3) for Ne, Ar, Kr and Xe target species. In particular, consideration of the window (4.4. 3.5–5.2) for CO^{2+}–Ar indicates that processes leading to the formation of quartet CO^+ states (fig. 1c) are favoured. For CO^{2+}–He, however, no accessible reaction channels occur within the window (5.7, 4.5–6.9). Consequently, as already noted, the cross section for this system is significantly lower than for any of the other rare gas target systems examined. Widths of calculated reaction windows (≈2 eV) appear to be much narrower than suggested by our experimental data.

We conclude that extension of the reaction window model, derived for atomic ion–atom systems, is applicable to some degree to this diatomic dication–atom single-electron capture series. Naturally, other reaction mechanisms, such as multisurface crossings at small internuclear separations, and Demkov transitions [27], are of considerable importance in interpreting endothermic and near-resonant channels.

Acknowledgement

One of the authors (ZH) gratefully acknowledges a stipend under the auspices of the Royal Society–Czechoslovak Academy of Sciences Exchange Program. We also acknowledge support of this work by the University College of Swansea. PJ thanks SERC for a postgraduate research studentship, and both SERC and the Mass Spectrometry Research Unit for a travel award to visit Prague.

References

[1] D. Smith, N.G. Adams, E. Alge, H. Villinger and W. Lindinger, J. Phys. B13 (1980) 2787, and references therein.
[2] K. Okuno, T. Koizumi and Y. Kaneko, Phys. Rev. Letters 40 (1978) 1708.
[3] J.B. Hasted, S.M. Iqbal and M.M. Yousaf, J. Phys. B4 (1971) 343.
[4] T. Ast, J.H. Beynon and R.G. Cooks, J. Am. Chem. Soc. 94 (1972) 6611.
[5] B.A. Huber, J. Phys. B13 (1980) 809.

[6] Y.Y. Makhdis, K. Birkinshaw and J.B. Hasted, J. Phys. B9 (1976) 111.
[7] B. Friedrich and Z. Herman, Chem. Phys. Letters 107 (1984) 375.
[8] D. Neuschäfer, Ch. Ottinger, S. Zimmerman, W. Lindinger, F. Howorka and H. Störi, Intern. J. Mass Spectrom. Ion Phys. 28 (1979) 345.
[9] E.Y. Kamber, P. Jonathan, A.G. Brenton and J.H. Beynon, J. Phys. B, to be published.
[10] K. Vekey, A.G. Brenton and J.H. Beynon, J. Phys. Chem. 90 (1986) 3569.
[11] D. Mathur, R.G. Kingston, F.M. Harris, A.G. Brenton and J.H. Beynon, J. Phys. B20 (1987) 1811.
[12] F.H. Dorman and J.D. Morrison, J. Chem. Phys. 35 (1961) 575.
[13] A.S. Newton and A.F. Sciamanna, J. Chem. Phys. 53 (1970) 132.
[14] E. Hille and T. Märk, J. Chem. Phys. 69 (1978) 4600.
[15] B. Brehm and G. De Frenes, Intern. J. Mass Spectrom. Ion Phys. 26 (1978) 251.
[16] A.C. Hurley, J. Chem. Phys. 54 (1971) 3656.
[17] J.M. Curtis and R.K. Boyd, J. Chem. Phys. 80 (1984) 1150.
[18] R.W. Wetmore, R.J. LeRoy and R.K. Boyd, J. Phys. Chem. 88 (1986) 6318.
[19] K.O. Huber and G. Herzberg, Spectroscopic constants of diatomic molecules (Van Nostrand Reinhold, New York, 1979).
[20] C.E. Moore, Atomic energy levels, Natl. Bur. Std. No. 457 (US Govt. Printing Office, Washington, 1949).
[21] R.P. Morgan, J.H. Beynon, R.H. Bateman and B.N. Green, Intern. J. Mass Spectrom. Ion Phys. 28 (1978) 171.
[22] E.Y. Kamber, D. Mathur and J.B. Hasted, J. Phys. B15 (1982) 263.
[23] T.F. Moran, F.C. Petty and A.F. Hedrick, J. Chem. Phys. 51 (1969) 2112.
[24] V. Čermák and Z. Herman, Coll. Czech. Chem. Commun. 30 (1965) 1343.
[25] K.C. Smyth, J.A. Schiavone and R.S. Freud, J. Chem. Phys. 60 (1974) 1358.
[26] M. Kimura, T. Iwai, Y. Kaneko, N. Kobayashi, A. Matsumoto, S. Ohtani, K. Okuno, S. Takagi, H. Tawara and S. Tsurubuchi, J. Phys. Soc. Japan 53 (1984) 2224.
[27] Y.N. Demkov, Zh. Eksp. Teor. Fiz. 45 (1963) 195.